98-3160

LA-UR- 3160

Approved for public release; distribution is unlimited.

Title: NUMERICAL MODELING OF SHEAR BAND FORMATION IN PBX-9501

CONF-980803--

Author(s): T. N. Dey, J. R. Kamm

Submitted to: 11th Int'l Detonation Symp., Snowmass, CO
Aug. 31 - sept. 4, 1998

DISTRIBUTION OF THIS DOCUMENT IS UNLIMITED

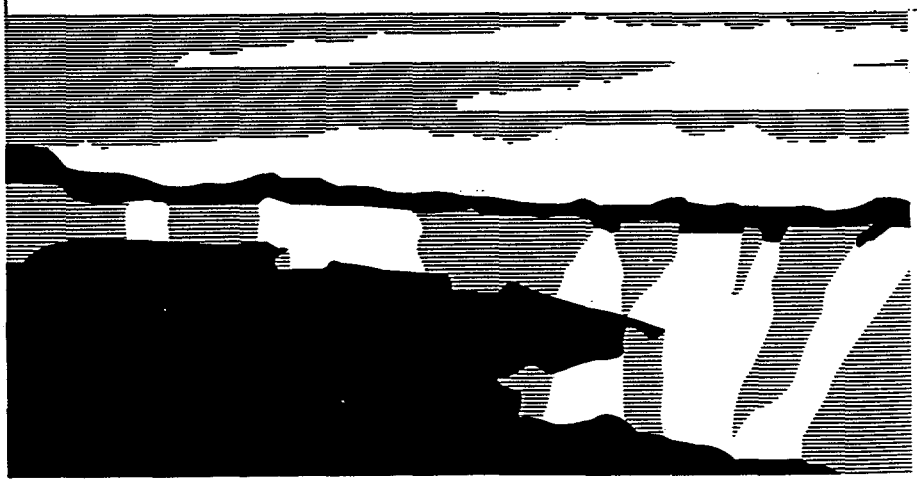

MASTER

Los Alamos
NATIONAL LABORATORY

DISCLAIMER

DISCLAIMER

Portions of this document may be illegible in electronic image products. Images are produced from the best available original document.

LA-UR- 98-3160

NUMERICAL MODELING OF SHEAR BAND FORMATION IN PBX-9501

T. N. Dey and J. R. Kamm
Los Alamos National Laboratory
Hydrodynamic Methods Group
Mail Stop D413
Los Alamos, NM USA 87545-1663

Adiabatic shear bands in explosives may be a source of ignition and lead to detonation. Three possible mechanisms leading to shear banding are (1) thermal softening, (2) mechanical softening due to microcracking, and (3) quasi-granular constitutive response. The latter two mechanisms can lead to shear band formation in PBXs at nominal strains much smaller than those required for the thermal softening mechanism. We study formation of shear bands with models including the latter two mechanisms under unconfined compression. Statistical variation of numerical results is similar to that observed in some experiments. However, the commonly used methods of calibrating constitutive models can be misleading because of effects due to shear band formation. One model currently being used for studies of shear band formation and ignition in PBX 9501 was calibrated in this way and may need re-examination.

INTRODUCTION

Thermal softening as a cause of shear band formation in materials has been extensively studied. Such adiabatic shear bands in explosives may be a source of ignition and lead to detonation [4,5,6,9,10,17]. At low to moderate deformation rates, two other mechanisms can also give rise to shear bands, and they require only small strains to do so. By concentrating deformation, these mechanisms may accelerate the formation of adiabatic shear bands.

One of these mechanisms is mechanical softening caused by microcracking, which may occur in the grains, in the binder, or at the grain-binder interface of plastic bonded explosives (PBXs) [3]. The other is a constitutive response characterized by a non-associated flow rule, as is observed in granular material such as soil[11]. In PBX-9501, insufficient experimental data on the constitutive behavior is available at this time to assess the roles that each of these mechanisms play at deformation rates of 10–1000 s^{-1}. In this paper we describe numerical studies in which the behavior of each mechanism is modeled, in order to guide an experimental program to characterize more accurately this material.

A preliminary constitutive model for PBX-9501, constructed by Johnson[8] to fit available data, generates shear bands by softening associated with microcracking. This model simulates visco-elastic behavior of the material caused by the estane/plasticizer binder. Coupled to this is a simplified statistical crack model, based on the work of Dienes[4] which generates softening behavior that sets in at 1–2% strain in this brittle composite explosive. This softening leads to shear band formation at nominal strain rates at and below 1000 s^{-1}. Shear band formation is suppressed at higher strain rates, since the rate of softening is limited by the finite maximum crack growth rate[3].

Brittle behavior at small strains, together with the granular nature of the HMX explosive component and the small weight-fraction of binder, suggest that constitutive behavior may be similar to that for solids. Unfortunately, the experimental data to test this hypothesis are not yet available for PBX-9501 or PBX-9502. Trumel, et al.[15] do report on constitutive model work for a non-reactive simulant for a propellant containing energetic grains bound by 10-20% synthetic rubber. Their model development is based on experiments of Cagnoux [2]. Their model requires a pressure-dependent yield surface together with volumetric compaction effects. This model is consistent with some phenomenology associated with granular materials such as sand. These results encourage us to examine the behavior of sand, where a non-associated flow rule is appropriate[12]. Our examination reveals characteristics that may be present in experiments on PBXs. Calculations using a model for sand suggest shear band formation at strain rates of 1000 s^{-1} and below. Although there is no intrinsic softening in this particular constitutive model, yet shear bands begin forming before the peak stress is obtained, i.e., while still hardening. This behavior stands in contrast to the thermal and mechanical softening mechanisms.

Both of these proposed mechanisms are sensitive to perturbations induced by material heterogeneity and heterogeneous loading. Indeed, in calculations with both homogeneous material and stress, no shear bands form.

Understanding shear band formation and its consequences requires models that properly account for

phenomenology found in experiments. Proper model calibration to simple laboratory experiments is the first step. In this paper, we undertake to examine stress-strain and localization phenomenology of two constitutive models in the context of unconfined compression tests on simple cylindrical samples. This type of test provides frequently used data at strain rates from quasi-static in a loading frame to a few thousand per second in a split-Hopkinson bar.

Since localization into shear bands is triggered by some form of perturbation, either material or stress heterogeneity, we examine the influence of these types of perturbations on the macroscopic stress-strain curves and macroscopic fracture pattern. We compare the macroscopic stress-strain curves to the ideal material response to determine how well the macroscopic curves can be used for model calibration.

MATERIAL RESPONSE MODELS

The visco-elastic microcracking constitutive model used here separates the material response into volumetric and deviatoric components [3,8]. The volumetric response is characterized by a constant bulk modulus appropriate for low-pressure regimes considered herein. The deviatoric response consists of two components acting in series: a visco-elastic response and a microcrack growth response. The visco-elastic behavior is characterized by N Maxwell elements, which act in parallel. The nth Maxwell element is modeled by expressing the deviatoric stress rate $\dot{s}_{ij}$ in terms of the deviatoric stress s_{ij}, the deviatoric strain rate $\dot{e}_{ij}$, the shear modulus G, and the relaxation time τ as:

$$\dot{s}_{ij}^{(n)} = 2G^{(n)}\dot{e}_{ij}^{(n)} - \frac{s_{ij}^{(n)}}{\tau^{(n)}}$$

where the superscript (n) denotes the nth element. Due to the parallel coupling of the visco-elastic elements, for deformations occurring more rapidly than the characteristic time of a given element, that element adds its stiffness to the other elements; for deformations occurring more slowly than the characteristic time, the element adds no stiffness.

The deviatoric strain due to cracking is related to the crack dimensions and the deviatoric stress as

$$2Ge_{ij}^{(c)} = (c/a)^3 s_{ij}$$

where c is the actual (evolving) crack radius and a is the characteristic (fixed) crack radius. With the total deviatoric strain rate equal to the sum of the visco-elastic deviatoric strain rate and the cracking deviatoric strain rate , the deviatoric strain rate in each visco-elastic element can be expressed as

$$\dot{s}_{ij}^{(n)} = 2G^{(n)}\dot{e}_{ij} - \frac{s_{ij}^{(n)}}{\tau^{(n)}} - \frac{G^{(n)}}{G}\left[3\left(\frac{c}{a}\right)^2\frac{\dot{c}}{a}s_{ij} + \left(\frac{c}{a}\right)^3\dot{s}_{ij}\right].$$

Summing the contributions of all elements gives the total deviatoric stress rate as

$$\dot{s}_{ij} = \left[2G\dot{e}_{ij} - \sum_{n=1}^{N}\frac{s_{ij}^{(n)}}{\tau^{(n)}} - 3\left(\frac{c}{a}\right)^2\frac{\dot{c}}{a}s_{ij}\right] \Big/ \left[1+(c/a)^3\right].$$

The model for crack evolution is given by

$$\dot{c} = \begin{cases} v_{\max}\left(K/K_1\right)^m, & K < K' \\ v_{\max}\left(1-\left(K_0/K\right)^2\right)^m, & K > K'. \end{cases}$$

In this expression, K is the stress intensity factor

$$K = \sqrt{\pi c}\,\sigma_{eff}$$

where σ_{eff} is the total effective stress, K_0 is the threshold stress intensity factor, and K_1 and K' are related through the following relations

$$K' = K_0\sqrt{1+(2/m)}$$

and

$$K_1 = K_0\sqrt{1+(2/m)}\left[1+(2/m)\right]^{1/m}.$$

The parameter m is chosen to insure continuity of the crack growth rate between the low strain rate, diffusion-controlled limit ($K \ll K_0$) and the high-strain rate limit where inertial effects are important ($K \gg K_0$) .

PBX-9501 is assigned a density of 1830 kg m^{-3} and a bulk modulus of 11.4 GPa. Data for PBX-9501 have been fitted to a visco-elastic model consisting of five elements; the values of the shear modulus $G^{(n)}$ and inverse relaxation time $1/\tau^{(n)}$, n=1,...,5, for PBX-9501 are provided in Table 1. Values for the initial crack radius c, the characteristic crack length a, the maximum crack growth rate $\dot{c}_{max}$, the fracture toughness K_0 , and the crack growth velocity exponent m are given in Table 2.

Element	1	2	3	4	5
Shear Modulus (GPa)	0.9440	0.1739	0.5212	0.9085	0.6875
Time Constant (s^{-1})	0.0	7.32E+3	7.32E+4	7.32E+5	2.00E+6

Table 1. Visco-elastic model parameters for PBX-9501.

We use a second constitutive model developed by Leroy and Ortiz [12] to examine the phenomenology associated with granular materials. This model for sand is based on the Drucker-Prager yield surface including a non-associated flow rule together with hardening from an initial to an ultimate yield surface.

Initial Crack Radius (m)	Char'c Crack Radius (m)	Max. Crack Speed ($m\ s^{-1}$)	Threshold Fracture Toughness ($GPa\ m^{-3/2}$)	Crack Growth Exponent
3.E-6	1.E-3	300	5.E-4	10

Table 2. Crack model parameters for PBX-9501.

This is a much simpler model than that employed by Trumel et al.[15]; however, the localization characteristics of the Leroy and Ortiz model have been studied extensively. The initial internal friction angle provides a yield surface that increases approximately three times more rapidly as a function of pressure than the Trumel et al. model.

The yield surface is described by:

$$Y = \alpha (P - P_0)$$

where $\alpha = 6 \sin \phi / (3 - \sin \phi)$

and $\sin \phi = \sin \phi_i + \sin \phi_m \cdot \gamma / (\gamma + \gamma_c)$.

Here, γ is equivalent plastic strain and P is pressure. The parameters used with this model are a density of 1600 kg m^{-3}, Young's modulus E = 2.0 GPa, Poisson ratio ν = 0.25, initial internal friction angle $\phi_i = 10°$, additional internal friction $\phi_m = 25°$, critical plastic strain $\gamma_c = 0.005$, and $P_0 = 10^{-4}$ GPa. A Prandtl flow rule, which is a non-associated flow rule for this model, is also used.

COMPUTATIONAL CONFIGURATION

A series of idealized plane strain calculations was performed at a strain rate of 100 s^{-1} and with varying perturbations. This strain rate is typical of those for which a non-shock initiation mechanism may induce a violent HE reaction. The prototype problem was chosen with dimensions similar to the commonly used unconfined compression experiment. The mesh extent is 0.0125 m horizontally by 0.0250 m vertically, with 25 cells in the horizontal direction and 50 cells vertically; the dimension of the initially square cells is 0.0005 m on a side. Mesh refinement studies show this mesh size is just small enough to resolve shear bands that may form.

Appropriate symmetry boundary conditions are assigned to the top and left boundaries so that the mesh corresponds to one-fourth of a typical experimental sample. The top boundary is displaced vertically, with no lateral constraint, at a constant velocity chosen to give a nominal strain rate of 100 s^{-1}. The left boundary is allowed to have free tangential slip but constrained to have no normal displacement; the right boundary is a free surface. Additionally, a uniform initial vertical velocity gradient is imposed throughout the mesh as a means to inhibit initial ring-up. As found in previous work[3], these transient waves can themselves cause a sufficient stress perturbation to trigger localization. Three different bottom boundary conditions are considered, all constrained to have no normal displacement: (1) frictionless, i.e., free tangential slip, (2) frictional tangential slip with a friction coefficient of 1.0, or (3) welded (i.e., constrained to allow no tangential displacement). The first and third of these conditions are idealized extremes of the lubricated and end conditions frequently employed in experiments, while the second condition approximates a state intermediate to those limits.

Calculations similar to these were performed by Shuttle and Smith [14]. They examined changes in stress-strain behavior due to different end constraint conditions for a material model with a Tresca yield condition and an associated flow rule subject to quasi-static loading and using a single perturbation to trigger shear band formation. Our calculations differ in choice of material models, strain rate and examination of distributions of perturbations.

Perturbations to the material properties are introduced to "seed" the shear band growth. While not directly modeling any known or proposed fluctuations in HE, these perturbations are intended to give some indication of the phenomenology in real PBXs. These perturbations consist of randomly chosen zones constituting 1%, 5%, 10% or 20% of the entire mesh. Figure 1 shows the mesh with perturbations applied to 10% of the cells.

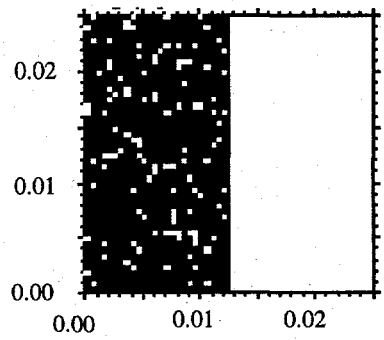

Figure 1. Initial grid for calculations with one realization of 10% inhomogeneity distribution. White zones represent perturbed material.

For the visco-elastic microcracking model the imposed perturbation consists of a fivefold increase in the initial crack radius, from c_0=3x10^{-6} m to c_0=15x10^{-6} m. For the Drucker-Prager model the perturbation includes changes to both the initial internal friction angle, decreased from $\phi_i = 10°$ to $\phi_i = 5°$, and to the additional internal friction angle, decreased from $\phi_m = 25°$ to $\phi_m = 15°$.

The cells to receive the perturbation are chosen according to a pseudo-random number generator. Between six and ten sets of perturbations were generated for each total volume and a computation was performed for each of them for each combination of boundary condition and material model. We have computed the

mean and standard deviation for each combination. Figure 2 shows average stress strain curves for each of the ten realizations of a 5% level of inhomogeneity for the Drucker-Prager model with welded boundary. These macroscopic stress-strain curves are volume averages of longitudinal stress and longitudinal strain over the sample. They correspond to the values found in experiments from load cell and loading platen displacement measurements. Figure 3 shows the corresponding mean stress-strain curve and one standard deviation bounds on the stress-strain curve. Hereinafter we will use these derived curves for presentation and discussion of results.

Calculations are performed for 2D plane strain conditions. Although axisymmetric conditions are typically used to match the prototype, this symmetry condition inhibits shear localization for models with non-associated flow rule and no intrinsic softening

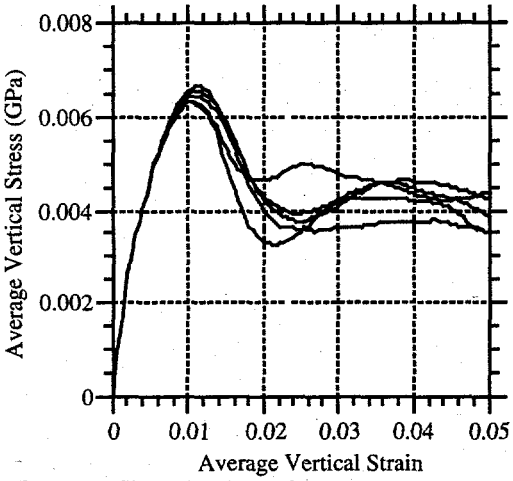

Figure 2. Six realizations of the stress-strain response for the Drucker-Prager model with welded boundary conditions and 5% inhomogeneity.

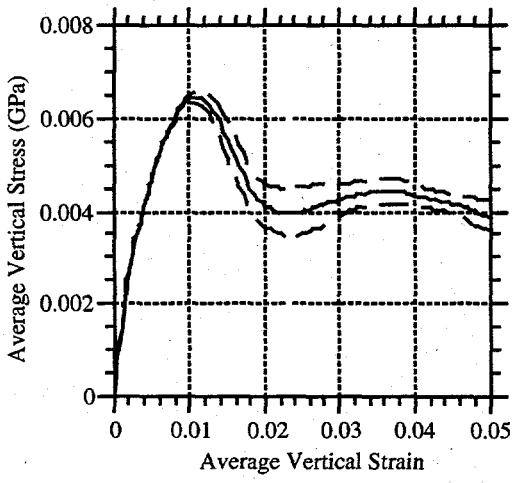

Figure 3. Mean stress response (solid line) plus-or-minus one standard deviation (dashed line) vs. strain for the Drucker-Prager model realizations shown in Figure. 2 (welded boundary conditions and 5% inhomogeneity).

mechanism[13]. Experiments on cylindrical samples, such as those by Idar et al.[7] discussed elsewhere in this paper, lose their apparent axisymmetry when shear localization occurs and the samples are broken into a number of non-axisymmetric pieces. Images in the Idar et al.[7] report show generally planar shear fractures frequently defining a prominent wedge of material at the sample ends. It is reasonable to use a plane strain model to study this phenomenology. The problem, however, is three-dimensional and we plan to continue our work with three-dimensional calculations.

RESULTS

Figures 2 and 3 show the "sample-to-sample" variability that can be generated by random perturbations when using the particular Drucker-Prager model employed here. The perturbations are insufficient to cause any variation in the stress-strain curve during the initial loading. It is only when shear localization begins that the "sample-to-sample" variability is generated. For this particular model, this leads to variations of about 15-20% of the peak stress magnitude at strains beyond the peak stress.

Figure 4 shows mean and one standard deviation curves for a series of calculations using the visco-elastic microcracking model. Compared to the Drucker-Prager model, the variability observed in calculations with the visco-elastic micracking model is quite small, being only about 5-10% of the peak stress magnitude.

Recently published high quality data by Idar et al.[7] provide interesting comparisons to these results. Their data is for unconfined quasi-static compression of cylindrical samples of PBX-9502. Since the models in our work are intended for PBX-9501, one must avoid over interpreting these comparisons. In their results, sample-to-sample variability is negligible at strains less than or equal to that at which the peak stress is reached.

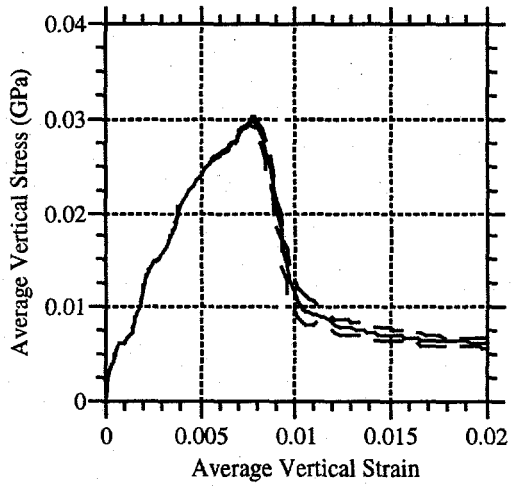

Figure 4. Mean stress response (solid line) plus-or-minus one standard deviation (dashed line) vs. strain for the visco-elastic microcracking model with welded boundary conditions and 10% inhomogeneity.

For greater strains than produce localization and a stress drop, sample-to-sample variability is approximately 25-30% of the peak stress. In this regard, the Drucker-Prager model behavior corresponds more closely.

Computational results suggest that both material property perturbations and stress perturbations due to sample end conditions can significantly alter macroscopic stress-strain response. Figure 5a-c shows results for the visco-elastic microcracking model as a function of volume fraction of perturbed material. As this figure shows, the first few percent perturbations cause the greatest reduction of peak stress, with increasing volumes of perturbed material resulting in a smaller rate of peak stress reduction. Additionally, the fewer the perturbations, the more steeply the stress drops as strain increases beyond the peak stress point. At low levels of inhomogeneity only a few well-defined shear bands develop. At high levels of inhomogeneity, shear bands are pervasive and sample deformation is macroscopically more homogeneous.

Figure 6 shows results for 1% inhomogeneity with the visco-elastic microcracking model as a function of the end constraint condition. The free-slip end condition, which provides no lateral constraint at the sample ends, leads to the highest peak stress. A frictional end constraint, with a friction coefficient of one, produces only an insignificantly lower peak stress. A welded end condition, which allows no lateral expansion of the sample end, produces a notable reduction in peak stress and in the stress-strain curve. In the latter case, the end constraint produces a stress perturbation that acts to trigger shear localization more effectively than the material perturbations being modeled. The peak stress reduction due to the welded end condition is approximately equal to that introduced by a 5% level of inhomogeneity. At greater levels of inhomogeneity, the difference among results for different end conditions is reduced.

The experiments of Idar et al.[7] include cases with frictional end constraint as well as lubricated ends. Peak stresses with frictional end constraints were equal to or slightly higher than for lubricated ends. This trend is opposite to that computed for the visco-elastic microcracking model.

Results obtained with the Drucker-Prager model offer similarities and differences to the visco-elastic microcracking model results. Figure 7 shows results for different inhomogeneity levels for calculations applying a frictional end constraint. The trend of peak stress reduction with increasing levels of inhomogeneity is similar. High levels of inhomogeneity lead to stress-strain curves with a relatively small stress reduction beyond the peak stress.

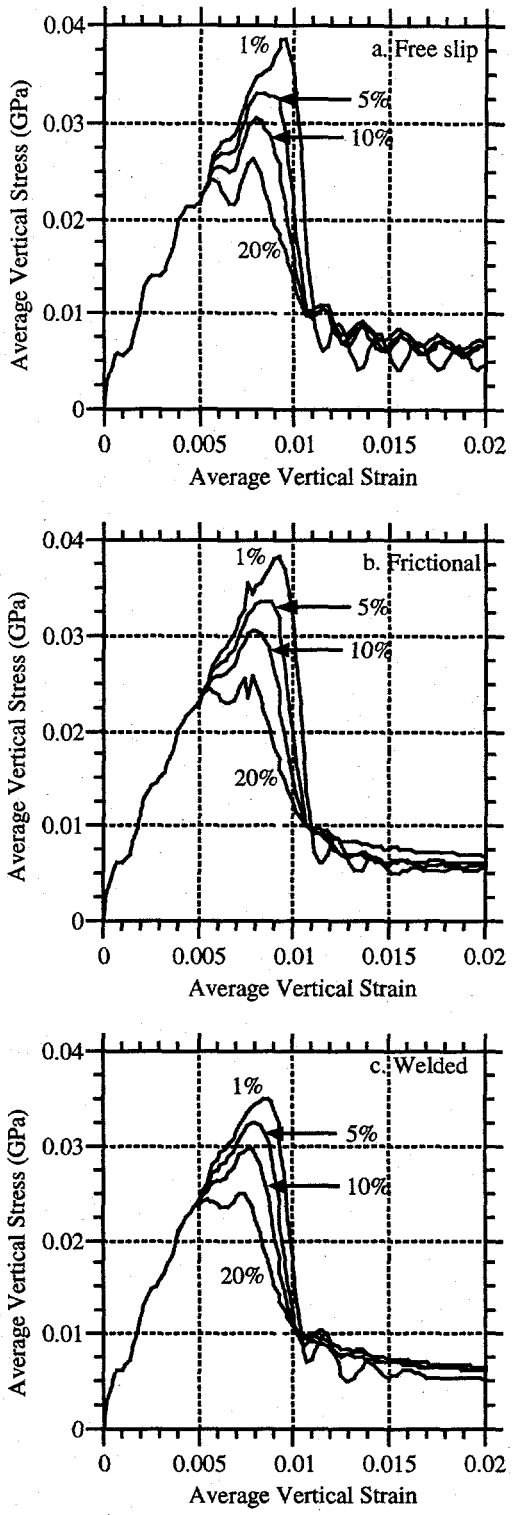

Figure 5. Mean vertical stress as a function of strain for the visco-elastic microcracking model with varying inhomogeneity. The top plot (a) shows results for the free slip boundary, the middle plot (b) for the frictional boundary, and the bottom plot (c) for the welded boundary.

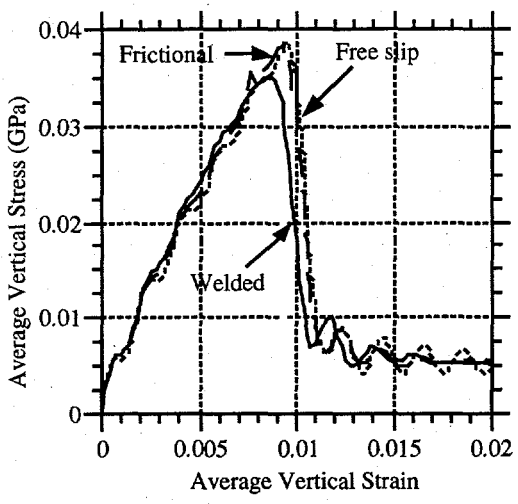

Figure 6. Mean vertical stress as a function of strain for the Johnson model with 1% inhomogeneity. The three curves represent the three boundary conditions: free slip (dotted), frictional (dashed), and welded (solid).

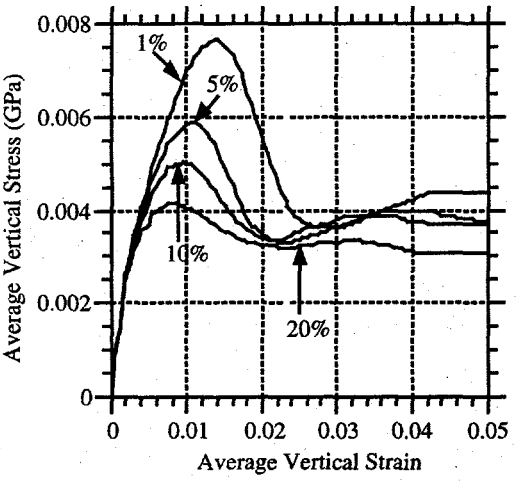

Figure 7. Stress-strain response for the Drucker-Prager model with frictional boundary conditions and varying degree of inhomogeniety.

Figure 8 shows results for peak stress as a function of inhomogeneity level and end constraint for the Drucker-Prager model. Figure 9 shows results for strain to failure, defined here as strain to peak stress. At all levels of inhomogeneity, the peak stress increases as end constraint changes from none (dotted line) to frictional constraint (dashed line) to welded constraint (solid line). This trend is the opposite to that found for the visco-elastic microcracking model, where increasing end constraint reduced peak stress. This is the same trend however, albeit of much larger magnitude, as observed in the experiments of Idar et al.[7]. Moreover, strain to failure increases with end constraint, but decreases as inhomogeneity increases. The strain to failure trend is opposite to that observed by Idar et al.[7] The result that peak stress varies linearly with log of inhomogeneity is notable, but may be serendipitous. It requires further scrutiny however, since for inhomogeneity levels greater than 50%, the original material and perturbing material interchange roles so that one would expect peak stress to approach that of the model used for perturbations.

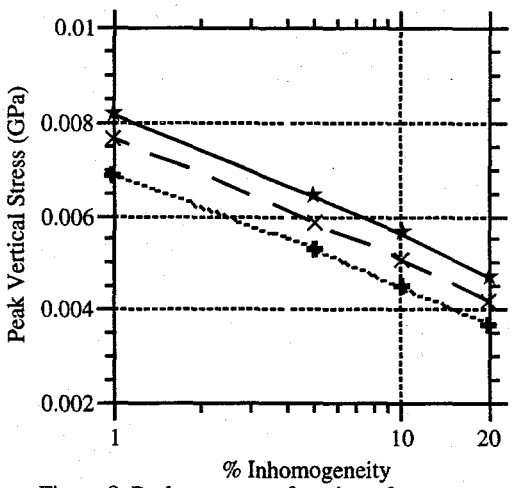

Figure 8. Peak stress as a function of percentage inhomogeneity for the Drucker-Prager model. The three curves represent the three boundary conditions: free slip (dotted), frictional (dashed), and welded (solid).

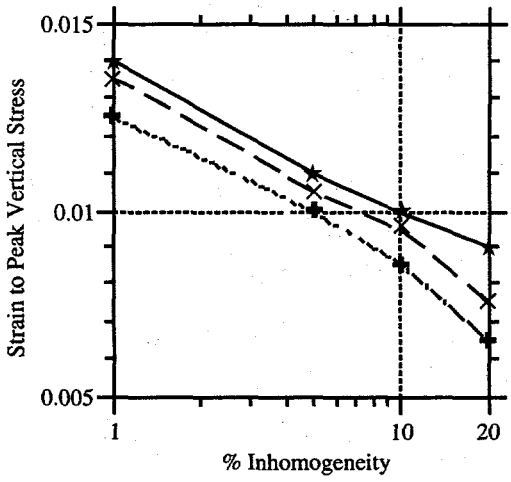

Figure 9. Strain to peak stress as a function of percentage inhomogeneity for the Drucker-Prager model. The three curves represent the three boundary conditions: free slip (dotted), frictional (dashed), and welded (solid).

The peak stress increase accompanying increasing end constraint results from the pressure-dependent yield surface in the Drucker-Prager model: end constraint leads to a higher mean stress (pressure) in the sample and a higher strength.

DISCUSSION

As constitutive models are being developed and used to study non-shock initiation of explosives, it becomes important to understand the localization behavior of explosives. Consequently, understanding the corresponding phenomena in the experiments used to calibrate these models becomes crucial.

Throughout this series of calculations, perturbations of material properties or stress state are imposed. These results show how macroscopic behavior can change dramatically due to shear band localization triggered by these perturbations even without any change in the intrinsic material model behavior. This observation is most evident from the results with the Drucker-Prager model. The intrinsic behavior of this material will not lead to brittle-type behavior (defined here as strain softening). The presence of perturbations triggers localization of deformation into shear bands, which give rise to the apparent macroscopic strain-softening behavior. The visco-elastic microcracking model used here displays a strong strain softening behavior intrinsically. The macroscopic behavior of this model is affected by both stress and material perturbations, although not to the extent of Drucker-Prager model used here.

Previous work using other material models at quasi-static loading rates showed the common practice of using the average stress-strain behavior as representative of the intrinsic material response is misleading when shear localization occurs [14,16]. Our results indicate that this will also be true at moderate strain rates with material models that may be suitable for PBXs. Other, more difficult, model calibration procedures are required[16]. The calibration for the visco-elastic microcracking model was originally done using macroscopic results from samples that exhibited shear localization without accounting for the consequences of this localization. Our results indicate this calibration is misleading and should be re-examined.

Considerations of localization and perturbation phenomenology on how a material model is developed and calibrated depend on the model's intended use. For models intended for the study of small strain problems where localization is unlikely, our results show that the average stress-strain behavior matches the intrinsic behavior of the material. In this case, the model will not be exercised in the regime where misleading results are likely to be obtained.

Similarly, for problems where localization is likely to be pervasive and the details of individual localization zones are unimportant, using the average stress-strain behavior will lead to a model that represents the average material response. While such a model would be unrepresentative of the intrinsic behavior, it is quite adequate for its intended use. While not in the constitutive model regime, reactive burn models for detonation wave propagation are a familiar example of this. Reactive burn models attempt to capture the representative response of a volume of material that may contain a distribution of hot spots. The bulk behavior is key since there is insufficient time in a detonation for hot spots to communicate and for one to grow at the exclusion of others.

For localization problems that do not fall in either of the above categories, our results demonstrate that use of average stress-strain data for a model fit may lead to misleading results. In all our results, average stress-strain results differ, in some case dramatically, from the intrinsic material model behavior. For use in estimating whether a shear band that may lead to HE ignition, such models will likely be unreliable.

Some experiments, such as those of Asay and co-workers[1], are under way that are intended to study in detail the formation of shear bands, their ignition, and the spread of combustion. The experiments that lead to ignition generally include an imposed strong stress perturbation, such as that by a punch. Localization is likely to be controlled by this imposed perturbation. As discussed above, models intended for studying such experiments would be unreliable if they are calibrated to the average stress-strain response in typical compression tests. Such compression tests, including the frictional end constraints, could provide an important validation of a material model. The ability to adequately predict the shear localization at the ends of this relatively simple test samples should be one level of qualification for models intended for study of the more complicated experiments.

CONCLUSIONS

We have examined the phenomenology of formation of shear bands in an experimental configuration, the unconfined compression test on cylindrical samples, commonly used for calibrating material constitutive models. Our results, as well as results of others using different material models, indicate that commonly used calibration procedures for models may be misleading when the samples display shear localization, as do the PBXs of interest in this study. Other, more complex, model calibration procedures are required[16]. The unconfined compression experiments with frictional end-constraint present appear to provide a viable validation experiment for constitutive models intended for study of other more complex experiments related to HE safety under non-shock conditions.

ACKNOWLEDGEMENTS

This work was performed under the auspices of Los Alamos National Laboratory which is operated by the University of California for the U.S. Department of Energy under contract W-7405-ENG-36.

REFERENCES

1. Asay, B. W., Laabs, G. W., Henson, B. F. & Funk, D. J. Speckle Photography During Dynamic Impact of an Energetic Material Using Laser Induced

Fluorescence *J. Appl. Phys.*, **82**(3), pp. 1093-1099, (1997).

2. Cagnoux, J. Dynamic Behavior of a Filled Polymer, *Journal de Physique, Colloque C3*, **49**, pp. C3-521-528 (1988).

3. Dey, T. N. & Johnson, J. N. Shear Band Formation in Plastic Bonded Explosive (PBX), *Proceedings of the 1997 Conference of the APS Topical Group on Shock Compression of Condensed Matter*, pp. 285-288 (1998).

4. Dienes, J. K. On Reactive Shear Bands, *Phys. Lett. A* **118**, pp. 433–437 (1986).

5. Field, J. E., Swallowe, G. M. & Heavens, S. N. Ignition mechanisms of explosives during mechanical deformation, *Proc. R. Soc. Lond. A* **382**, pp. 231–244 (1981).

6. Frey, R. B. The Initiation of Explosive Charges by Rapid Shear, *Proceedings of the Seventh Symposium (International) on Detonation*, pp. 36–42 (1981).

7. Idar, D. J., R. L. Rabie, and P. D. Scott. Quasi-static, Low-strain Rate Compression Measurements of Thermally Treated and Mechanically Insulted PBX 9502 Samples, Los Alamos National Laboratory Report LA-UR-97-5116 (1997).

8. Johnson, J. N. Private communication (1996).

9. Kerrisk, J. F. A Model for Shear-Band Formation and High-Explosive Initiation in a Hydrodynamics Code, Los Alamos National Laboratory Report LA-13127 (1996).

10. Krishna Mohan, V., Jyothi Bhasu, V. C. & Field, J. E. Role of Adiabatic Shear Bands in Initiation of Explosives by Drop-weight Impact, *Proceedings of the Ninth Symposium (International) on Detonation*, pp. 1276–1283 (1989).

11. Lade, P. V., Nelson, R. B. & Ito, Y. M. Instability of Granular Materials with Nonassociated Flow, *J. Eng. Mech.*, **39** (2), pp. 2173–2191 (1988).

12. Leroy, Y. and M. Ortiz. Finite Element Analysis of Transient Strain Localization in Frictional Solids, *Int. J. Num Anal. Methods in Geomechanics*, **14**, pp. 93-124 (1990).

13. Rudnicki, J. W. & Rice, J. R. Conditions for the localization of deformation in pressure-sensitive dilatant materials, *J. Mech. Phys. Solids* **23**, pp. 371–394 (1975).

14. Shuttle, D. A. and I. M. Smith. Numerical simulation of shear band formation in soils, *Int. J. Num. Anal. Meth. Geomech.*, **12**, pp. 611-626 (1988).

15. Trumel, H., A. Fanget, and A. Dragon. A Finite Strain Elastic-Plastic Model for the Quasi-static Behavior of Particulate Composites, *Int. J. Engng. Sci.*, **34**, pp. 677-698 (1996).

16. Vardoulakis, I. and B. Graf. Calibration of constitutive models for granular materials using data from biaxial experiments, *Geotechnique*, **35**(3), pp. 299-317 (1985).

17. Winter, R. E. & Field, J. E. The role of localized plastic flow in the impact initiation of explosives, *Proc. R. Soc. Lond.*, **A343**, pp. 399–413 (1975).